


Enhancing the biofuel upgrade performance for Pd nanoparticles *via* increasing the support hydrophilicity of metal–organic frameworks†

Qi Sun, Meng Chen, Briana Aguila, Nicholas Nguyen and Shengqian Ma *

Received 15th January 2017, Accepted 27th January 2017

DOI: 10.1039/c7fd00015d

In this work, the influence of the hydrophilic/hydrophobic nature of metal–organic framework (MOF) materials on the catalytic performance of supported Pd nanoparticles for biofuel upgrade was studied. We show that the introduction of hydrophilic groups on a MOF can greatly enhance the performance of the resultant catalyst. Specifically, Pd nanoparticles supported on MIL-101–SO₃Na with superhydrophilicity (Pd/MIL-101–SO₃Na) far outperforms pristine MIL-101 and the benchmark catalyst Pd/C in the hydrodeoxygenation reaction of vanillin, a model component of pyrolysis oil derived from the lignin fraction. This is attributed to a favorable mode of adsorption of the highly water soluble reactants on the more hydrophilic support in the vicinity of the catalytically active Pd nanoparticles, thereby promoting their transformation.

Introduction

Activity and selectivity in heterogeneous catalysis are highly determined by the catalyst surface properties.¹ The control over the surface wettability of heterogeneous catalysts offers an exceptional opportunity in regulating the interaction between substrates and catalysts and thus the activity and selectivity.² For example, hydrophilic catalyst surfaces facilitate the enrichment of the corresponding substrates and expulsion of the hydrophobic products, with beneficial consequences for catalytic conversion. From another aspect, to secure the future energy supply and to manage the global warming issue arising from the greenhouse effect, energy from renewable sources is desired to be increased relative to the use of fossil-based fuels.³ Unfortunately, biofuels derived from the pyrolysis of renewable biomass have a low energy density, immiscibility with conventional fuels, and instability over time, due to the high amount of oxygen components involved.

Department of Chemistry, University of South Florida, 4202 E. Fowler Avenue, Tampa, FL 33620, USA. E-mail: sqma@usf.edu

† Electronic supplementary information (ESI) available. See DOI: 10.1039/c7fd00015d

Therefore, efficient removal of oxygen from the biofuel is essential if they are to be fully used.⁴ Given the hydrophilicity of the oxygen-contained substrate and hydrophobicity of the corresponding deoxygenated products, it is thus postulated that increasing the hydrophilicity of the catalyst can promote the transformations.

During the past decade, metal–organic frameworks (MOFs)⁵ have captured enormous attention due to their potential versatility in applications such as gas adsorption and storage,⁶ sensing,⁷ opto-electronics,⁸ catalysis,⁹ and many more.¹⁰ The tunable composition and structure architecture, in conjunction with the high crystallinity and open framework of MOFs, make it possible to not only precisely control the nature, density, and spatial arrangement of the active centers, but also serve as an auspicious platform for guest encapsulation for designing efficient catalysts. MOFs have been extensively studied with metal nanoparticles (MNPs) for their potential application as heterogeneous catalysts.¹¹ In these cases, MOFs served as supports to stabilize MNPs by virtue of their high internal surface area and large pore volume, that provide spatial confinement to restrict the growth of MNPs and prevent the active particles from aggregating, and their channels can facilitate the mass transfer for the reactants and products. However, less effort has been made to take advantage of the combination of the chemical amenability and porous structure of MOFs for MNPs stabilization and activity modification. Many interesting issues are worthy of being exploited on this topic. In particular, the tunable functionality in the MOFs would impart them with adjustable wettability, which, if being employed for biofuel upgrade, would be of great significance.

To illustrate our design, herein, chromium terephthalate MIL-101 (hereafter denoted as MIL-101) was chosen as a wettability controllable MOF support for immobilizing MNPs due to its high water/chemical stability, functionalizable pore walls, large surface area, and two giant zeotypic cavities with free diameters of 2.9 and 3.4 nm accessible through two pore windows of 1.2 and 1.6 nm.¹² This study is an example of how the performance of metal catalysts can be precisely designed *via* adjusting the wettability of the MOF supports by chemical modification, as exemplified by Pd supported on MIL-101 and sodium sulfonate ($-\text{SO}_3\text{Na}$) functionalized MIL-101 (MIL-101- SO_3Na). We chose vanillin (4-hydroxy-3-methoxybenzaldehyde), a large component of pyrolysis oil derived from the lignin fraction,¹³ as a typical reactant to demonstrate the important role of catalyst wettability on the catalytic hydrodeoxygenation reaction. Remarkably, the catalytic performance of Pd nanoparticles supported on MIL-101- SO_3Na with superhydrophilicity (Pd/MIL-101- SO_3Na) far outperforms pristine MIL-101 and the benchmark catalyst Pd/C. The enrichment of a highly water soluble reactant (vanillin) and intermediate (vanillin alcohol) in conjugation with the decreased adsorption of the hydrophobic target product (2-methoxy-4-methylphenol) on the catalyst surface, avoiding the blockage of active sites, accounts for the observed excellent performance of the Pd/MIL-101- SO_3Na catalyst. These findings give insight to a design concept for catalysts to promote biofuel upgrade.

Experimental

Materials

Solvents were purified according to standard laboratory methods. Dichloromethane was distilled over CaH_2 . Other commercially available reagents were purchased in high purity and used without further purification.

Catalyst synthesis

Synthesis of MIL-101. MIL-101 was synthesized according to a previously reported method.¹⁴

Synthesis of MIL-101-SO₃Na. First, MIL-101-SO₃H was synthesized by a post-synthetic modification strategy as reported in the literature.¹⁵ In a typical run, 500 mg of activated MIL-101 was dispersed in 20 mL of dichloromethane at 0 °C. Then 0.15 g of chlorosulfonic acid (ClSO₃H) dissolved in 10 mL dichloromethane was added drop-wise to the mixture under stirring. After 30 min, the solid product was separated by filtration, washed with water and acetone, and soaked in ethanol for 24 h at 70 °C. After being filtrated and dried under vacuum, the resultant material was denoted as MIL-101-SO₃H. The MIL-101-SO₃Na was obtained by ion exchange of MIL-101-SO₃H with excess 0.1 M NaCl aqueous solution.

Synthesis of Pd/MIL-101. Pd/MIL-101 catalyst was prepared by a simple impregnation method. Briefly, 200 mg of MIL-101 was added to 20 mL of deionized water under stirring, followed by the addition of 14 mg of Na₂PdCl₄. After being stirred at room temperature for 24 h, the pH value of the mixture was adjusted to 8–9 by NaOH aqueous solution and then NaBH₄ was introduced. The mixture was filtrated, washed thoroughly with water, and dried under vacuum at 50 °C to afford the title material. Inductively coupled plasma-optical emission spectrometry (ICP-OES) results revealed that the Pd loading amount in Pd/MIL-101 was 2.4 wt%.

Synthesis of Pd/MIL-101-SO₃Na. Pd/MIL-101-SO₃Na was synthesized similarly to that of Pd/MIL-101 except that MIL-101-SO₃Na was used instead of MIL-101. ICP-OES results revealed that the Pd loading amount in Pd/MIL-101-SO₃Na was 2.5 wt%.

Catalytic tests

As a model reaction for biofuel upgrade, the hydrodeoxygenation of vanillin was studied. Typically, 0.152 g (1 mmol) of vanillin, 10 mL of H₂O, and the catalyst were sealed in a 50 mL Schlenk flask with a magnetic stirrer. After being evacuated, the system was purged with H₂ using a balloon. The tube was placed in a preheated oil bath and stirred for a desired time. After reaction, the reactant and product were extracted by ethyl acetate and the conversion and yield of the reaction were analyzed by GC-MS or ¹H NMR.

For each catalyst recycling, the catalysts were separated by centrifugation, washed with acetone and water, and used directly for the next run.

Characterization

Powder X-ray diffraction (PXRD) data were collected on a Bruker AXS D8 Advance A25 Powder X-ray diffractometer (40 kV, 40 mA) using Cu K α ($\lambda = 1.5406 \text{ \AA}$) radiation. The gas adsorption isotherms were collected on the surface area analyzer, ASAP 2020. The N₂ sorption isotherms were measured at 77 K using a liquid N₂ bath. Transmission electron microscopy (TEM) images were obtained using a JEM 2100F instrument. IR spectra were recorded on a Nicolet Impact 410 FTIR spectrometer. ICP-OES was performed on a Perkin-Elmer Elan DRC II Quadrupole instrument. X-ray photoelectron spectroscopy (XPS) was performed on a Thermo ESCALAB 250 with Al K α irradiation at $\theta = 90^\circ$ for X-ray sources, and

the binding energies were calibrated using the C 1s peak at 284.9 eV. ^1H NMR spectra were recorded on a Bruker Avance-400 (400 MHz) spectrometer. Chemical shifts are expressed in ppm downfield from tetramethylsilane (TMS) at $\delta = 0$ ppm, and J values are given in Hz. Photographs of water drops on the surface of the samples in the pressed pellet form were measured with SL200KB (USA KNO Industry Co.), equipped with a CCD camera.

Results and discussion

Given the hydrophilicity of biofuel, to increase the water wettability and thereby to increase the affinity of MIL-101 towards biofuel, sodium sulfonate ($-\text{SO}_3\text{Na}$) was chosen as the chemical functionality to be introduced. MIL-101- SO_3Na can be obtained by the treatment of MIL-101 with ClSO_3H in dichloromethane using procedures detailed in the literature,¹⁵ followed by ion exchange with excess NaCl aqueous solution. The crystallinity of the resultant MIL-101- SO_3Na was examined by PXRD, which gave sharp diffraction lines matching those of the pristine MIL-101 pattern (Fig. 1a). This clearly indicates preservation of the MIL-101 structure during the post-synthetic process. The successful grafting of $-\text{SO}_3\text{Na}$ groups onto MIL-101 was confirmed by X-ray photoelectron spectroscopy (XPS) and FT-IR studies. The XPS spectrum of MIL-101- SO_3Na revealed a sulfur signal at a binding energy of 169.0 eV, verifying the post-synthetic modification occurrence (Fig. 1b). In addition, the FT-IR spectrum of MIL-101- SO_3Na showed the characteristic band of $\text{O}=\text{S}=\text{O}$ at 1225, 1166, and 1078 cm^{-1} compared with the MIL-101, confirming the existence of $-\text{SO}_3\text{Na}$ groups (Fig. 1c).¹⁵ N_2 sorption isotherms collected at 77 K (Fig. 1d) revealed a decrease in the BET surface area after conversion of MIL-101 ($2454 \text{ m}^2 \text{ g}^{-1}$) to MIL-101- SO_3Na ($1868 \text{ m}^2 \text{ g}^{-1}$). To investigate the surface wettability of MIL-101 and MIL-101- SO_3Na , they were dispersed at the interface of a biphasic solution, in which the upper layer was ethyl acetate and the bottom was water. Interestingly, MIL-101 prefers to stay in the organic phase, while MIL-101- SO_3Na is well dispersed in the water phase (Fig. 1e), thus indicating that the introduction of the sodium sulfonate group greatly enhances the hydrophilicity of MIL-101. This phenomenon is supported by the contact angle results, which show that the air-water contact angles on the surface of MIL-101 and MIL-101- SO_3Na are 75° and $<5^\circ$, respectively (Fig. 1f and g).

Given the high porosity and different hydrophilic/hydrophobic nature of MIL-101 and MIL-101- SO_3Na , they may be suitable for loading Pd nanoparticles (NPs) to investigate the effect of catalyst wettability on the performance of catalyzing biofuel upgrade. Therefore, Pd NPs were loaded by a simple incipient-wetness impregnation method. The actual contents of Pd NPs in all catalysts were evaluated by ICP-OES. The resultant materials exhibit PXRD profiles that closely match those of as-prepared MIL-101 and MIL-101- SO_3Na , and no diffraction peak for Pd NPs can be detected in both the Pd/MIL-101 and Pd/MIL-101- SO_3Na materials (Fig. S1, ESI[†]), revealing that the Pd NPs are likely very small. This assumption is consistent with the results of TEM observation, which present highly dispersed and fine Pd NPs with sizes of around 2–3 nm in the resultant materials (Fig. 2a and b). To study the chemical state of the Pd species on MIL-101 and MIL-101- SO_3Na , XPS spectroscopy was performed. The XPS spectra show that the Pd 3d binding energies in Pd/MIL-101 and Pd/MIL-101- SO_3Na are almost the

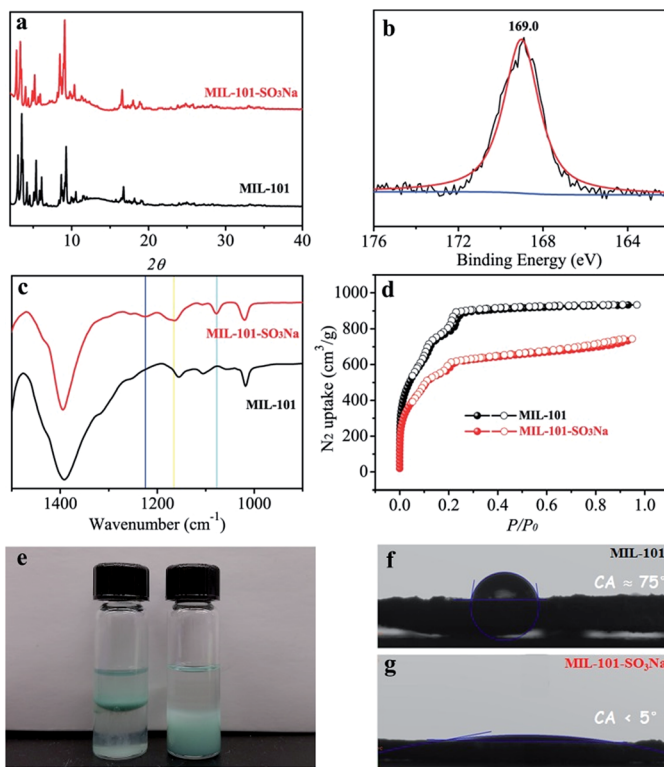


Fig. 1 (a) XRD patterns, (b) S 2p XPS spectrum, (c) IR spectra, (d) N₂ sorption isotherms collected at 77 K, (e) photos of MIL-101 (left) and MIL-101–SO₃Na (right) dispersed in a biphasic solution of ethyl acetate (upper) and water solution (bottom), and (f) and (g) air–water contact angles.

same (Fig. 2c and d), giving Pd 3d_{3/2} and Pd 3d_{5/2} binding energies at around 340.2 and 335.0 eV, respectively, indicating that most of the Pd species in these materials are in the metallic form (Pd⁰).¹⁶

Notably, the wettability of MIL-101 and MIL-101–SO₃Na after loading Pd species is not an obvious change, as demonstrated by the fact that Pd/MIL-101 and Pd/MIL-101–SO₃Na are still inclined to stay in the ethyl acetate phase and water phase, respectively (Fig. 3, inset). In addition, BET measurements of Pd/MIL-101 and Pd/MIL-101–SO₃Na suggest the retention of the porosity of MIL-101 and MIL-101–SO₃Na, giving rise to surface areas as high as 2139 m² g^{−1} and 1629 m² g^{−1}, respectively (Fig. S2, ESI†).

With the Pd/MIL-101 and Pd/MIL-101–SO₃Na catalysts exhibiting different hydrophilicity, we tested their activity towards biofuel upgrade in aqueous medium. Given the importance of deoxygenated lignin-derived pyrolysis oil, we used vanillin,¹³ a common component of pyrolysis oil derived from the lignin fraction, as a model substrate to explore the principal hydrogenation and deoxygenation routes. In a typical run, the reactions were carried out in a Schlenk tube purged with atmospheric H₂ using a balloon, vanillin as a reactant and water as the solvent in the presence of the catalyst at 100 °C. Vanillin alcohol was produced

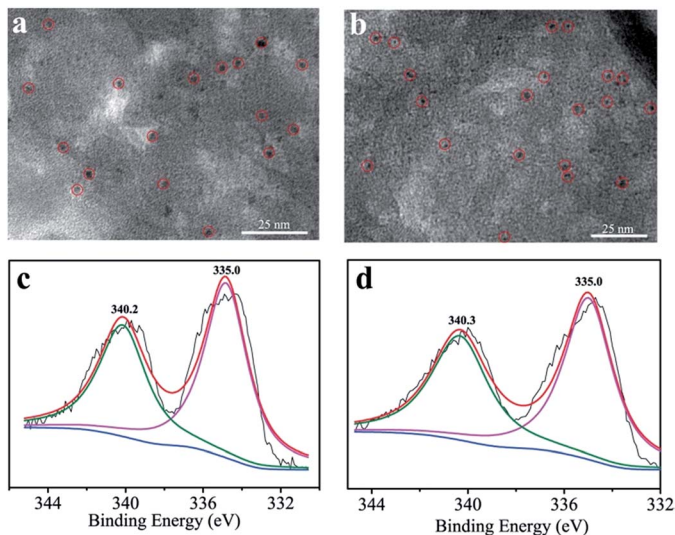


Fig. 2 (a) and (b) TEM images of Pd/MIL-101 and Pd/MIL-101-SO₃Na, respectively, and (c) and (d) Pd 3d XPS spectra of Pd/MIL-101 and Pd/MIL-101-SO₃Na, respectively.

as an intermediate and 2-methoxy-4-methylphenol was the objective product. Remarkably, Pd/MIL-101-SO₃Na showed exceptional catalytic activity, giving rise to a 2-methoxy-4-methylphenol yield as high as 99%, which clearly outperformed Pd/MIL-101 tested under identical conditions, which afforded vanillin alcohol and 2-methoxy-4-methylphenol yields of 23% and 77%, respectively. To give more information, the reaction pathway was investigated by tracing the product distribution change along with the reaction time of the Pd/MIL-101 and Pd/MIL-101-SO₃Na, respectively. Fig. 3 displays the evolution of the reagent and product concentration of the Pd/MIL-101 and Pd/MIL-101-SO₃Na catalysts. Both of the catalysts exhibit similar trend profiles except that Pd/MIL-101-SO₃Na shows faster kinetics, implying that the catalytic transformation underwent the same pathway. Specifically, reactions were accompanied by a rapid increase in vanillin alcohol and a decrease in vanillin, illustrating that vanillin is mainly hydrogenated to vanillin alcohol in the first step. However, even in the first 30 min, 2-methoxy-4-

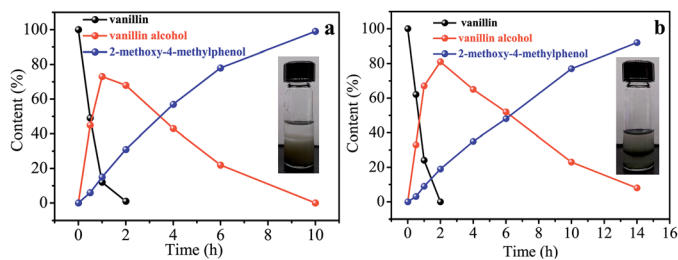


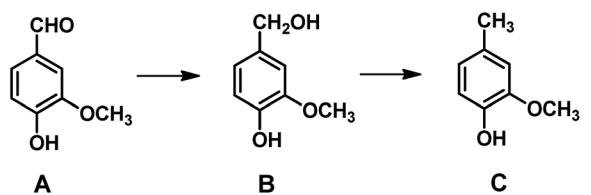
Fig. 3 Evolution of reactant and product concentrations with reaction time over (a) Pd/MIL-101-SO₃Na and (b) Pd/MIL-101. Insets are the photos of corresponding catalyst dispersed in a biphasic solution of ethyl acetate (upper) and water solution (bottom).

methylphenol was observed, suggesting that hydrogenolysis of vanillin alcohol occurred or that vanillin underwent direct hydrogenolysis of C=O as well. Later, hydrogenolysis of vanillin alcohol proceeded smoothly and almost all of the vanillin alcohol was converted to 2-methoxy-4-methylphenol.

Considering the similar loading amount and size of the Pd NPs on MIL-101 and MIL-101-SO₃Na, the higher activity and better selectivity for the Pd/MIL-101-SO₃Na catalyst than those over the Pd/C catalyst are mainly attributed to the better wettability of the reactant to the Pd/MIL-101-SO₃Na catalyst than that to the Pd/MIL-101 catalyst (Fig. S3, ESI†). The superhydrophilic Pd/MIL-101-SO₃Na catalyst is favorable for the adsorption of hydrophilic oxygen-rich reactants (*e.g.* vanillin) and desorption of the hydrophobic hydrodeoxygenated product (2-methoxy-4-methylphenol). This feature would shift the reaction balance, thereby leading to a significant enhancement of the catalytic performance. To provide additional proof for our deduction, a hydrophobic benchmark catalyst, Pd/C, was employed, affording vanillin alcohol and 2-methoxy-4-methylphenol yields of 28% and 72%, respectively (Table 1, entry 3), which is inferior to Pd/MIL-101-SO₃Na in terms of selectivity.

Given the importance of catalyst stability, XRD and TEM analyses were performed for the Pd/MIL-101-SO₃Na after the catalytic reaction (Fig. S4, ESI†). The structural intactness of the MOF framework as well as the metallic Pd states remain unchanged, as confirmed by the PXRD and XPS patterns, respectively. TEM measurements of the used Pd/MIL-101-SO₃Na catalyst showed no significant changes in the size and morphologies of the Pd NPs. These results suggest the robustness of Pd/MIL-101-SO₃Na, thereby implying its potential recyclability. To assess the performance of Pd/MIL-101-SO₃Na as a regenerable catalyst, a cycling experiment was conducted. After one reaction run, the catalyst was

Table 1 Catalytic performance of the hydrodeoxygenation of vanillin in aqueous solution over various catalysts^a



| Entry | Catalyst | Conv. (%) A | Yield (%) | |
|----------------|-------------------------------|----------------|-----------|----|
| | | | B | C |
| 1 | Pd/MIL-101-SO ₃ Na | >99 | Trace | 99 |
| 2 | Pd/MIL-101 | >99 | 23 | 77 |
| 3 ^b | Pd/C | >99 | 28 | 72 |
| 4 ^c | Pd/MIL-101-SO ₃ Na | >99 | Trace | 99 |
| 5 ^c | Pd/MIL-101 | >99 | 54 | 46 |

^a Reaction conditions: the mixture of vanillin (1 mmol, 0.152 g), H₂O (10 mL), and catalyst (2 mol% based on the Pd) was stirred at 100 °C under H₂ (1 atm) for 10 h. ^b Palladium on active carbon (5 wt% Pd) was bought from Acros (CAS: 7440-05-3). ^c Vanillin (2 mmol, 0.304 g), H₂O (20 mL), catalyst (0.25 mol% based on the Pd) and reaction for 48 h.

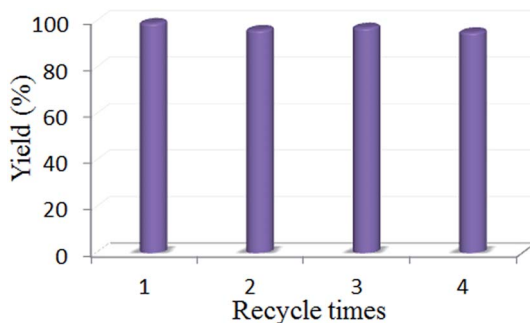


Fig. 4 Recycling tests of Pd/MIL-101-SO₃Na in the hydrodeoxygenation of vanillin. Reaction conditions are as given in Table 1.

collected through centrifugation and reused in the next run under the same conditions. It was found that after three consecutive cycles, Pd/MIL-101-SO₃Na was still highly active with the reaction yield of 2-methoxy-4-methylphenol maintaining up to 95% (Fig. 4).

For practical applications, both a high yield and low cost are required. We thus conducted the reaction with an increased vanillin/Pd (substrate/catalyst) molar ratio of S/C = 400. The disparity of Pd/MIL-101 and Pd/MIL-101-SO₃Na in terms of selectivity turns out to be larger. Pd/MIL-101-SO₃Na afforded the 2-methoxy-4-methylphenol with a yield of 99% within 48 h, while Pd/MIL-101 only gave a corresponding yield of 46% under identical conditions (Table 1, entries 4 and 5).

Conclusions

In summary, Pd NPs have been immobilized on MOFs with different degrees of hydrophilicity, showing high performance for the hydrodeoxygenation of vanillin, a common component in lignin-derived biofuel, under mild reaction conditions with water as a green solvent. It is found that the wettability of the MOF plays a crucial role in the catalytic activity of biofuel upgrade. The Pd NPs stabilized with MIL-101-SO₃Na with superhydrophilicity exhibits superior activity, clearly outperforming Pd/MIL-101 and the benchmark catalyst Pd/C. This is a good example to demonstrate the significance of the wettability of nanoporous materials for MNPs immobilization to promote catalytic conversion. Given the structural diversity and chemical tailorability of MOFs, there is a huge opportunity to achieve MOFs with tunable wettability, which would open a new avenue to enhance the catalytic performance of MNPs.

Acknowledgements

The authors acknowledge NSF (DMR-1352065) and the University of South Florida for financial support of this work.

Notes and references

- (a) L. Wang and F.-S. Xiao, *ChemCatChem*, 2014, **6**, 3048–3052; (b) F. Liu, L. Wang, Q. Sun, L. Zhu, X. Meng and F.-S. Xiao, *J. Am. Chem. Soc.*, 2012,

- 134, 16948–16950; (c) G. Huang, Q. Yang, Q. Xu, S.-H. Yu and H.-L. Jiang, *Angew. Chem., Int. Ed.*, 2016, **55**, 7379–7983; (d) Y. Dai, S. Liu and N. Zheng, *J. Am. Chem. Soc.*, 2014, **136**, 5583–5586; (e) M. Wang, F. Wang, J. Ma, C. Chen, S. Shi and J. Xu, *Chem. Commun.*, 2013, **49**, 6623–6625; (f) Q. Sun, B. Aguila, G. Verma, X. Liu, Z. Dai, F. Deng, X. Meng, F.-S. Xiao and S. Ma, *Chem*, 2016, **1**, 628–639.
- 2 (a) S. Crossley, J. Faria, M. Shen and D. E. Resasco, *Science*, 2010, **327**, 68–72; (b) Q. Sun, Y. Jin, L. Zhu, L. Wang, X. Meng and F.-S. Xiao, *Nano Today*, 2013, **8**, 342–350; (c) C. Tian, C. Bao, A. Binder, Z. Zhu, B. Hu, Y. Guo, B. Zhao and S. Dai, *Chem. Commun.*, 2013, **49**, 8668–8670; (d) Y. Liu, E. Lotero and J. G. Goodwin Jr, *J. Catal.*, 2006, **243**, 221–228; (e) K. Nakatsuka, K. Mori, S. Okada, S. Ikurumi, T. Kamegawa and H. Yamashita, *Chem.–Eur. J.*, 2014, **20**, 8348–8354; (f) R. W. Gosselink, W. Xia, M. Muhler, K. P. De Jong and J. H. Bitter, *ACS Catal.*, 2013, **3**, 2397–2402.
- 3 (a) V. G. W. Huber, S. Iborra and A. Corma, *Chem. Rev.*, 2006, **106**, 4044–4049; (b) D. Tilman, J. Hill and C. Lehman, *Science*, 2006, **314**, 1598–1600; (c) E. M. Rubin, *Nature*, 2008, **454**, 841–845; (d) C. Luo, S. Wang and H. Liu, *Angew. Chem., Int. Ed.*, 2007, **46**, 7636–7639; (e) H. Olcay, A. V. Subrahmanyam, R. Xing, J. Lajoie, J. A. Dumesic and G. W. Huber, *Energy Environ. Sci.*, 2013, **6**, 205–216.
- 4 (a) M. Stöcker, *Angew. Chem., Int. Ed.*, 2008, **47**, 9200–9211; (b) K. Yana, T. Lafleur, G. Wua, J. Liao, C. Cenga and X. Xie, *Appl. Catal., A*, 2013, 46852–46858; (c) M. Saidi, F. Samimi, D. Karimipourfard, T. Nimmanwudipong, B. C. Gates and M. R. Rahimpour, *Energy Environ. Sci.*, 2014, **7**, 103–129; (d) K. Yan, T. Lafleur, X. Wu, J. Chai, G. Wu and X. Xie, *Chem. Commun.*, 2015, **51**, 6984–6987.
- 5 (a) H.-C. Zhou and S. Kitagawa, *Chem. Soc. Rev.*, 2014, **43**, 5415–5418; (b) S. L. James, *Chem. Soc. Rev.*, 2003, **32**, 276–288; (c) H. Furukawa, K. H. Cordova, M. O’Keeffe and O. M. Yaghi, *Science*, 2013, **341**, 1230444; (d) Q. Sun, H. He, W.-Y. Gao, B. Aguila, L. Wojtas, Z. Dai, J. Li, Y.-S. Chen, F.-S. Xiao and S. Ma, *Nat. Commun.*, 2016, **7**, 13300.
- 6 (a) S. Ma and H.-C. Zhou, *Chem. Commun.*, 2010, **46**, 44–53; (b) M. P. Suh, H. J. Park, T. K. Prasad and D.-W. Lim, *Chem. Rev.*, 2011, **112**, 782–835; (c) T.-L. Hu, H. Wang, B. Li, R. Krishna, H. Wu, W. Zhou, Y. Zhao, Y. Han, X. Wang, W. Zhu, Z. Yao, S. Xiang and B. Chen, *Nat. Commun.*, 2015, **6**, 7328.
- 7 (a) J. Zhou, H. Li, H. Zhang, H. Li, W. Shi and P. Cheng, *Adv. Mater.*, 2015, **27**, 7072–7077; (b) Z. Hu, B. J. Deibert and J. Li, *Chem. Soc. Rev.*, 2014, **43**, 5815–5840.
- 8 (a) V. Stavila, A. A. Talin and M. D. Allendorf, *Chem. Soc. Rev.*, 2014, **43**, 5994–6010; (b) S. S. Park, E. R. Hontz, L. Sun, C. H. Hendon, A. Walsh, T. Van Voorhis and M. Dincă, *J. Am. Chem. Soc.*, 2015, **137**, 1774–1777.
- 9 (a) J. Liu, L. Chen, H. Cui, J. Zhang, L. Zhang and C.-Y. Su, *Chem. Soc. Rev.*, 2014, **43**, 6011–6061; (b) S. Saha, G. Das, J. Thote and R. Banerjee, *J. Am. Chem. Soc.*, 2014, **136**, 14845–14851; (c) K. Mo, Y. Yang and Y. Cui, *J. Am. Chem. Soc.*, 2014, **136**, 1746–1749; (d) Z. Li, R. Yu, J. Huang, Y. Shi, D. Zhang, X. Zhong, D. Wang, Y. Wu and Y. Li, *Nat. Commun.*, 2015, **6**, 8248.
- 10 (a) Y. Peng, T. Gong, K. Zhang, X. Lin, Y. Liu, J. Jiang and Y. Cui, *Nat. Commun.*, 2014, **5**, 4406; (b) B. Van de Voorde, B. Bueken, J. Denayer and D. De Vos, *Chem. Soc. Rev.*, 2014, **43**, 5766–5788; (c) P. Li, J. A. Modica, A. J. Howarth, L. E. Vargas,

- P. Z. Moghadam, R. Q. Snurr, M. Mrksich, J. T. Hupp and O. K. Farha, *Chem*, 2016, **1**, 1–16.
- 11 (a) Q.-L. Zhu and Q. Xu, *Chem*, 2016, **1**, 220–245; (b) Q.-L. Zhu, J. Li and Q. Xu, *J. Am. Chem. Soc.*, 2013, **135**, 10210–10213; (c) W. Zhang, G. Lu, C. Cui, Y. Liu, S. Li, W. Yan, C. Xing, Y. R. Cui, Y. Yang and F. Huo, *Adv. Mater.*, 2014, **26**, 4056–4060; (d) J.-D. Xiao, Q. Shang, Y. Xiong, Q. Zhang, Y. Luo, S.-H. Yu and H.-L. Jiang, *Angew. Chem., Int. Ed.*, 2016, **55**, 9389–9393; (e) K. M. Choi, K. Na, G. A. Somorjai and O. M. Yaghi, *J. Am. Chem. Soc.*, 2015, **137**, 7810–7816.
- 12 G. Férey, C. Mellot-Draznieks, C. Serre, F. Millange, J. Dutour, S. Surblé and I. Margiolaki, *Science*, 2005, **309**, 2040–2042.
- 13 (a) X. Xu, Y. Li, Y. Gong, P. Zhang, H. Li and Y. Wang, *J. Am. Chem. Soc.*, 2012, **134**, 16987–16990; (b) Y.-Z. Chen, G. Cai, Y. Wang, Q. Xu, S.-H. Yu and H.-L. Jiang, *Green Chem.*, 2016, **18**, 1212–1217; (c) Z. Lv, Q. Sun, X. Meng and F.-S. Xiao, *J. Mater. Chem. A*, 2013, **1**, 8630–8635; (d) X. Yang, Y. Liang, X. Zhao, Y. Song, L. Hu, X. Wang, Z. Wang and J. Qiu, *RSC Adv.*, 2014, **4**, 31932–31936; (e) Z. Zhu, H. Tan, J. Wang, S. Yu and K. Zhou, *Green Chem.*, 2014, **16**, 2636–2643; (f) A. Aijaz, Q.-L. Zhu, N. Tsumori, T. Akita and Q. Xu, *Chem. Commun.*, 2015, **51**, 2577–2580.
- 14 L. Bromberg, Y. Diao, H. Wu, S. A. Speakman and T. A. Hatton, *Chem. Mater.*, 2012, **24**, 1664–1675.
- 15 M. Saikia and L. Saikia, *RSC Adv.*, 2016, **6**, 15846–15853.
- 16 Z. Zhu, H. Tan, J. Wang, S. Yu and K. Zhou, *Green Chem.*, 2014, **16**, 2636–2643.